J Neurophysiol 90: 1737–1746, 2003.
First published April 30, 2003; 10.1152/jn.00180.2003.

Flash Photolysis Reveals a Diversity of Ionotropic Glutamate Receptors on the Mitral Cell Somatodendritic Membrane

Graeme Lowe
Monell Chemical Senses Center, Philadelphia, Pennsylvania 19104-3308

Submitted 26 February 2003; accepted in final form 24 April 2003

Lowe, Graeme. Flash photolysis reveals a diversity of ionotropic glutamate receptors on the mitral cell somatodendritic membrane. *J Neurophysiol* 90: 1737–1746, 2003. First published April 30, 2003; 10.1152/jn.00180.2003. It is widely held that the soma and basal dendrites of olfactory bulb mitral cells receive exclusively inhibitory synaptic input from local interneurons. However, the mitral somatodendritic membrane exhibits immunoreactivity for a variety of glutamate receptors, and blocking GABA receptors unmasks mitral cell self-excitation. This excitation is proposed to be mediated either by diffuse spillover of the mitral cells' own released glutamate, or by punctate transmission from glutamate-releasing granule cells. This study examined the pharmacology and kinetics of glutamate sensitivity of mitral cells by flash photolysis of nitroindoline caged glutamates, which facilitate reliable activation of receptors in the synaptic cleft. Wide-field laser uncaging (3.5-ms flash) of approximately 0.5–1 mM glutamate onto the soma activated large currents with fast (3.4-ms rise, 7.5-ms decay) and slow (64-ms rise, >10-s decay) components. In 100 μM APV, slow currents were reduced to 53% of control (257-ms rise, 2-s decay), displayed outward rectification in 1.3 mM Mg^{2+}, and blocked by 15 μM 5,7-dichlorokynurenate. Responses to $\lesssim$100 μM glutamate were fully antagonized by 100 μM APV, consistent with competitive inhibition at high-affinity NMDA receptors. An APV-resistant NMDA receptor was not observed, refuting the punctate transmission model. Fast currents were blocked by 10 μM NBQX, boosted 3.28-fold by 100 μM cyclothiazide, and resolved into AMPA (40%) and kainate (60%) receptor components by 100 μM SYM2206. The results suggest that self-excitation depends on AMPA, kainite, and conventional NMDA autoreceptors on the mitral cell.

INTRODUCTION

Mitral cells constitute the main output neurons of the olfactory bulb. Their activity is under the control of synaptic inputs directed onto their apical (primary) dendrites, and onto their somata and basal (secondary) dendrites. The primary dendrites extend to the glomerular layer of the bulb, where they arborize as distal tufts receiving direct contact from convergent axonal projections of olfactory receptor cells. Glutamate release from receptor cell terminals drives strong excitation of the apical tufts by activating both AMPA/kainate and NMDA classes of ionotropic receptors on the postsynaptic membrane (Berkowicz et al. 1994; Ennis et al. 1996; Sassoe-Pognetto et al. 1993). The secondary dendrites radiate widely across a deep dendritic zone, the external plexiform layer. The membrane of the soma and secondary dendrites receives powerful GABAergic inhibition from granule cell dendrites by reciprocal synaptic contacts (Isaacson and Strowbridge 1998; Jahr and Nicoll 1980; Rall et al. 1966). At these synapses, granule cell spines, activated by glutamate released from the mitral cell, can mediate negative feedback dendrodendritic inhibition of a mitral cell's own activity, as well as lateral inhibition of one mitral cell by another.

Assigning the roles of excitation and inhibition to separate dendrites simplifies the computational task of a cell. However, synaptic input to the primary dendrite is not purely excitatory, but includes dendrodendritic inhibition at the tuft by juxtaglomerular cells (Getchell and Shepherd 1975; Schoppa and Westbrook 2002). This local inhibition may be regarded as modifying the excitation patterns relayed from the glomerulus to the mitral soma by the primary dendrite. There are also inhibitory $GABA_A$ receptors expressed on the more proximal trunk of the primary dendrite that may further regulate its excitability (Lowe 2002). Thus, although the principal role of the primary dendrite is to relay excitatory signals to the soma, these signals are subject to modification by inhibitory synapses.

In contrast to the primary dendrite, it has been widely accepted that fast synaptic input to the soma and secondary dendrites of mitral cells is exclusively inhibitory. This view was supported by electron microscopic studies on dendrodendritic synapses in the external plexiform layer, where the asymmetric junctions usually associated with excitatory connections were always oriented from mitral cells to interneuron spines (Price and Powell 1970b; Sassoe-Pognetto and Ottersen 2000). However, the mitral cell somatodendritic membrane exhibits positive immunoreactivity for ionotropic glutamate receptors, including subunits of AMPA/kainate (Montague and Greer 1999) and NMDA receptors (Giustetto et al. 1997), as well as metabotropic receptors (van den Pol 1995). The function of these receptors on the mitral cell is not fully understood. One hypothesis postulates that the ionotropic receptors operate as autoreceptors for detecting glutamate released from the mitral cell (Aroniadou-Anderjaska et al. 1999; Friedman and Strowbridge 2000; Salin et al. 2001). The NMDA receptors may also be capable of participating in spillover transmission between adjacent synapses (Isaacson 1999). Recently, the conventional view of exclusively inhibitory transmission was challenged by the report of punctate transmission at fast dendrodendritic excitatory synapses linking mitral and granule cells (Didier et al. 2001). Because of their novelty, the existence of

Address for reprint requests: G. Lowe, Monell Chemical Senses Center, 3500 Market St., Philadelphia, PA 19104-3308 (E-mail: loweg@monell.org).

The costs of publication of this article were defrayed in part by the payment of page charges. The article must therefore be hereby marked "*advertisement*" in accordance with 18 U.S.C. Section 1734 solely to indicate this fact.

such synapses has been controversial. If confirmed, they would require the development of more complex models of information-processing circuits in the olfactory bulb.

The present study applied whole cell patch-clamp recording and photolysis of caged glutamate to investigate the types of ionotropic receptors responsible for the glutamate sensitivity of the mitral cell somatodendritic membrane. Cells in olfactory bulb slices were directly stimulated in situ by glutamate released by laser flash photolysis of new, highly stable caged precursors with negligible prephotolysis activity (Canepari et al. 2001). The latter property is a crucial requirement for avoiding background activation and desensitization of receptors. This approach is superior to the iontophoretic method used previously (Didier et al. 2001) because it overcomes the diffusion barrier of the synaptic cleft. The speed of caged release is also well suited for reliable activation of rapidly desensitizing AMPA/kainate receptors, and the stimulus magnitude can be estimated by calculation. The results show that mitral cell somatodendritic excitation depends on fast currents mediated by both AMPA and kainate receptors, and on slow currents mediated by high-affinity NMDA receptors. The slow currents were partially antagonized by APV at high glutamate concentrations, and fully antagonized at low concentrations. The effects of APV can be explained by competitive inhibition, without invoking the "APV-resistant" NMDA receptor, which was a key element of the punctate transmission model.

METHODS

Slice preparation and electrophysiological recording

Slice preparation and recording followed previously described protocols (Lowe 2002). Briefly, male rats (P21–28, CD, Charles River Breeding Laboratories, Houston TX) were killed by halothane anesthesia, and the olfactory bulbs removed into an ice-cold sucrose slicing solution containing (in mM): 240 sucrose, 2.5 KCl, 10 Na-HEPES, 10 glucose, 1 $CaCl_2$, 4 $MgCl_2$, 0.2 ascorbic acid, pH 7.2, bubbled with 100% oxygen. Horizontal slices (160 μm) were cut with a custom-built vibrating-blade tissue slicer (60 Hz, horizontal oscillation 1 mm, vertical oscillation <2 μm), and allowed to recover for 1–3 h (30–23°C) in an interface chamber with high Mg^{2+} artificial cerebrospinal fluid (ACSF) (in mM): 124 NaCl, 2.5 KCl, 26 $NaHCO_3$, 1.25 NaH_2PO_4, 10 glucose, 1 $CaCl_2$, 3 $MgCl_2$, bubbled with 95% O_2–5% CO_2. After recovery the solution in the interface chamber was switched to standard ACSF (in mM): 124 NaCl, 2.5 KCl, 26 $NaHCO_3$, 1.25 NaH_2PO_4, 25 glucose, 2 $CaCl_2$, 1.3 $MgCl_2$, bubbled with 95%-O_2–5% CO_2. During recording, slices were submerged and perfused at 2 ml/min with standard ACSF at 25°C, bubbled with 95% O_2, 5% CO_2. In some studies of NMDA receptors, $MgCl_2$ was omitted from the ACSF. Mitral cell somata were visualized with a Nikon E600 FN microscope equipped with a Leica 63X/NA 0.90 water immersion objective, and DIC optics.

Recordings were made from the soma under whole cell voltage-clamp, with pipettes (3–8 MΩ) filled either with a CsCl-based solution containing (in mM): 126.3 CsCl, 4.9 KCl, 25.2 K-HEPES, 0.2 K-EGTA, 1.9 Mg-ATP, 0.3 Na-GTP, 1 $MgCl_2$, 3.9 Na_2-phosphocreatine, 6.3 biocytin (pH 7.2, junction potential correction -5.6 mV); or a Cs-methanesulfonate–based solution containing (in mM): 130 Cs-$MeSO_3$, 5 NaCl, 24 Na-HEPES, 0.2 K-EGTA, 2 Mg-ATP, 0.3 Na-GTP, 1 $MgCl_2$, 4 Na_2-phosphocreatine, 6.5 biocytin (pH 7.2, junction potential correction -12.2 mV). Corrections for liquid junction potentials were made with the generalized Henderson equation using JPCalc software (Cell MicroControls, VA) (Barry 1994), taking the relative mobility of $MeSO_3$ as 0.58 (Ng and Barry 1995). Whole cell currents were recorded with a PC-ONE (Dagan) or an EPC-8 (HEKA Electronics) patch-clamp amplifier, and digitized at 50 kHz, 16-bit resolution by software written in LabVIEW (National Instruments). In all recordings, the bath contained 1 μM tetrodotoxin (TTX) to block regenerative sodium currents, 50 μM bicuculline methiodide (BMI; Sigma-RBI) to inhibit $GABA_A$ receptors, and 150 μM Cd^{2+} to block calcium channels. Other pharmacological agents used were: 15–30 μM 5,7-dichlorokynurenic acid (dCK; Sigma-RBI), 100 μM D-(−)-2-amino-5-phosphonopentanoic acid (APV; Sigma-RBI), 100 μM (±)-4-(4-aminophenyl)-1,2-dihydro-1-methyl-2-propylcarbamoyl-6,7-methylenedioxyphthalazine (SYM2206; Tocris), 10 μM 2,3-dioxo-6-nitro-1,2,3,4-tetrahydrobenzo[*f*]quinoxaline-7-sulfonamide (NBQX, disodium; Sigma-RBI), and 100 μM 6-chloro-3,4-dihydro-3-(2-norboren-5-yl)-2H-1,2,4-benzothiazidiazine-7-sulfonamide-1,1-dioxide [cyclothiazide (CTZ); RBI]. Because of their low aqueous solubility, stock solutions of the drugs dCK, SYM2206 and cyclothiazide were prepared in DMSO and added by dilution into ACSF (final DMSO 0.1, 0.2, and 0.5%, respectively, with DMSO added to control bath solutions). After all experiments, slices were fixed overnight in 2% glutaraldehyde, and the morphology of recorded cells was recovered by staining with Vectastain Elite ABC kit and a VIP peroxidase substrate kit (Vector Laboratories, Burlingame, CA).

Laser flash photolysis

The basic instrumentation and methods for flash photolysis were described in detail previously (Lowe 2002). In brief, slices were maintained in a recycling perfusion chamber (4.6 ml bubbled standard ACSF). Caged glutamate [1.15 mM 7-nitroindolinyl (NI) glutamate; 0.2, 0.5, or 1 mM 4-methoxy-7-nitroindolinyl (MNI) glutamate; Sigma-RBI and Tocris] and various pharmacological agents were introduced into recycled perfusion by injection into a loop manifold. The beam from an Innova 90C argon ion laser (multiline UV, 351–364 nm) (Coherent) was directed through the microscope fluorescence port, and reflected off a dichroic mirror (XF2031, Omega), which sent it through the DIC prism to be focused by the Leica 63X/NA 0.90 objective. Laser optics and microscope were moved across the preparation under computer control using a custom-built X-Y optical bench, and the focal plane was adjusted vertically with a piezoelectric translator (P-723, Polytec PI). For flash photolysis, the beam was gated by an electronic shutter (Uniblitz, Vincent Associates), with open time set to 3.5 ms.

At the focal plane, photolysis occurs in a very small spot with effective diameter <2.5 μm, and uncaging glutamate within such a small region of the soma evoked relatively small currents. To boost the signal, the total membrane area stimulated by glutamate was expanded by raising the focal plane to 100 μm above the soma, thereby exposing the cell to a wider beam. The focal plane was raised, not lowered, to avoid exposing the slice to intense radiation at the beam waist. Recorded mitral cell somata were not deeper than about 50 μm below the slice surface. The size and position of the beam at 100 μm were determined by observing the excited fluorescence of a thin layer (15 μm) of Lucifer yellow solution trapped between two coverlips. This defocused spot was imaged using a substage microscope constructed from a Zeiss Plan-NEOFLUAR 40X/NA 0.75 infinity-corrected objective, and a Zeiss Axiovert 35M tube lens. After blocking UV transmission with a 460-nm long-pass filter (XF3091, Omega), the fluorescent image was detected with a CCD camera (Hamamatsu C2400-79H, set to $\gamma = 1$), and captured by a frame grabber. The beam profile was well fit by a Gaussian function, and displayed excellent radial symmetry ($1/e^2$ radius along major and minor axes: $W_x = 17.44$ μm, $W_y = 16.95$ μm). In horizontal slices, the average mitral cell diameter is 20 μm along a transverse axis, and 30 μm along a vertical axis (Price and Powell 1970a), so a beam with diameter 34 μm would stimulate the soma and proximal portions of the primary and secondary dendrites.

The concentration of glutamate generated by a flash was estimated

from two models of photolysis by a Gaussian beam. The first model provided a simplified description with two variables: $P(z, t)$, the power at distance z from the objective, at time t, contained within the $1/e^2$ beam radius; and $C(z, t)$, the corresponding concentration of caged glutamate averaged over this beam radius. The radially averaged concentration at the end of a flash was obtained by integrating the equations

$$\frac{\partial p}{\partial \zeta} = -\left(\frac{z_0}{\lambda_{CG}} c + \frac{z_0}{\lambda_N}(1 - c) + \sum_i \frac{z_0}{\lambda_i}\right) p \tag{1}$$

$$\frac{\partial c}{\partial \tau} = -\frac{z_0}{\lambda} \frac{p}{1 + \zeta^2} c \tag{2}$$

expressed in terms of the dimensionless power and concentration variables

$$p(\zeta, \tau) = \frac{P(z, t)}{A_p A_{\text{obj}} P_0}, \quad c(\zeta, \tau) = \frac{C(z, t)}{C_0} \tag{3}$$

which are functions of the dimensionless space and time coordinates

$$\zeta = \frac{z - WD}{z_0}, \quad \tau = \frac{t}{\tau_{ph}} \tag{4}$$

The physical parameters include: the decay lengths $\lambda_{CG} = 1/2.303 E_{CG} C_0$, $\lambda_N = 1/2.303 E_N C_0$,, and $\lambda_i = 1/2.303 E_i C_i$, for optical absorption by caged glutamate, nitrosoindole photoproduct and ith pharmacological agent, respectively; and the time constant τ_{ph}, for photolysis at the beam waist, where uncaging is most rapid

$$\frac{1}{\tau_{ph}} = \frac{2.303 Q_p E_{CG}}{\epsilon_\lambda N_A} \frac{A_p A_{\text{obj}} P_0}{z_0^2} \tag{5}$$

The model parameters were as follows: E_{CG} and E_N are the molar extinction coefficients, at 360 nm, of the caged glutamate and nitrosoindole photoproduct, respectively; C_0 is the initial concentration of caged glutamate; E_i represents the molar extinction coefficients at 360 nm and C_i, the concentrations of the UV-absorbing pharmacological agents in the bath; Q_P is the quantum yield of caged glutamate; $\epsilon_\lambda = 5.52 \times 10^{-19}$ J, the photon energy at 360 nm; $N_A = 6.022 \times 10^{23}$ mol^{-1}; $\lambda = 360$ nm; $WD = 2.2$ mm, the objective working distance; $z_0 = \pi w_0^2/\lambda$ is the Rayleigh range for the Gaussian beam, where $w_0 = 0.668$ μm, the beam waist (at focal plane) corresponding to $W = 17.2$ μm at 100 μm below the waist; P_0 is the laser power; $A_P = 0.8$ is the UV attenuation factor of the DIC prism and $A_{\text{obj}} = 0.65$, the UV attenuation factor of the Leica objective (both attenuations of the laser beam were measured by a photodiode). The boundary and initial conditions for *Eqs. 1* and *2* were

$$\begin{aligned} p(z = 0, \tau) &= 0.86 P_0 A_P A_{\text{obj}} \\ c(\zeta, 0) &= 1 \end{aligned} \tag{6}$$

where the factor of 0.86 represents the fraction of total beam power carried inside the $1/e^2$ beam radius.

Equation 1 is the Beer–Lambert Law with a nonlinear coupling term representing dynamic optical absorption by the medium, as the caged glutamate is consumed and replaced by a more transparent photoproduct. The extinction coefficients at $\lambda = 347$ nm are (in M^{-1} cm^{-1}): for the NI-cage, $E_{CG} = 2720$ (Papageorgiou et al. 1999); for the MNI-cage, $E_{CG} = 4330$ (Papageorgiou and Corrie 2000); for the photoproducts, $E_N = 1400$ and 2660, respectively (J.E.T. Corrie, personal communication). At the termination of a 3.5-ms flash, beam power at the cell was typically about 15% higher than the initial power; in the results, the time-averaged power at the cell is quoted.

Equation 2 is a first-order kinetic description of photolysis, justified by the very rapid photorelease of glutamate with a time constant of about 200 ns, much shorter than the 3.5-ms duration of the flash (Morrison et al. 2002). The photolysis rate in *Eq. 2* scales with mean intensity, which is inversely proportional to the area bounded by $W(z)$, the $1/e^2$ radius of the Gaussian beam (Saleh and Teich 1991)

$$W(z) = w_0 \sqrt{1 + \left(\frac{z - WD}{z_0}\right)^2} \tag{7}$$

The quantum yields Q_P are 0.043 for the NI-cage (Papageorgiou et al. 1999) and 0.085 for the MNI-cage (Papageorgiou and Corrie 2000).

Equations 1 and *2* were integrated numerically by fourth-order Runge–Kutta, with 5.75-μm spatial grid and 5.8-μs time grid (400 × 600 points at uniform spacing; programs written in LabVIEW and Mathematica, Wolfram Research). On a coarser grid, the iterations diverged for some experimental parameters, and on a finer grid, the increase in accuracy was much less than experimental error (final calculated glutamate concentration increased by 0.0015% when grid spacing was halved). Numerical stability was improved when the temporal grid was set finer than the spatial grid. Typical calculated uncaging efficiencies were 49% at $P_0 = 24$ mW laser power (2.17 mW at the cell); 76% at 50 mW (4.63 mW) for 1.15 mM NI-cage; 68% at 24 mW (1.18 mW); 91% at 50 mW (2.55 mW) for 1 mM MNI-cage. When uncaging with a water immersion objective, the approximately twofold improvement in quantum yield of the MNI- over the NI-caging group was largely offset by its higher extinction coefficient. Beam passage through the solution of caged compound above the slice strongly attenuated the power, to 24% of input power for the NI-cage and 10% of input power for the MNI-cage. A single 3.5-ms flash at the highest laser power (50 mW) for the MNI-cage produced 17 pmol of glutamate integrated along the length of the beam, causing a 3.7-nM final concentration increment in the bath, after dilution into the total volume of the recycled perfusion solution. In all experiments, the total number of flashes was <50; therefore long-term desensitization of receptors by accumulation of glutamate in the bath (<200 nM) was not a problem.

The model with spatially averaged concentration provides a simple, convenient estimate of mean glutamate released, but does not tell the range of uncaged glutamate concentrations. The intensity profile of an unattenuated Gaussian beam varies from 31.4 to 232.6% of its mean value, from the $1/e^2$ edge to the center. Scaling P_0 over this range in the model suggests that glutamate concentrations may vary from about 40 to 150% of the mean value. The polar surfaces of the cell soma are exposed to the high end, and the equatorial surfaces and proximal dendrites to the low end of this range. The whole cell current is a spatial summation of membrane currents activated by glutamate over this concentration range. Errors in estimating the mean concentration may arise from nonlinearities resulting from depletion of caged glutamate and increased dynamic transparency in the center of the beam where the light intensity peaks. To account for these effects, a more accurate calculation was performed by incorporating a radial coordinate. Photolysis was computed along cylindrically symmetric pencils of rays, indexed in polar coordinates (ρ, z) by a radial "impact" parameter β

$$\rho = \beta \sqrt{1 + \left(\frac{z - WD}{z_0}\right)^2} \tag{8}$$

These rays are good approximations of wavefront normals for a narrow beam (measured divergence angle, 0.17 radians) in which wavefront curvature and phase lag are slowly varying functions of z (Saleh and Teich 1991). Photolysis along rays is described by

$$\frac{\partial u}{\partial \zeta} = -\left(\frac{z_0}{\lambda_{CG}} c + \frac{z_0}{\lambda_N}(1 - c) + \sum_i \frac{z_0}{\lambda_i}\right) \sqrt{\left(1 + \frac{\eta^2 \zeta^2}{1 + \zeta^2}\right)} u \tag{9}$$

$$\frac{\partial c}{\partial \tau} = -\frac{u}{1 + \zeta^2} c \tag{10}$$

where a dimensionless power variable was introduced in place of the light intensity, $I(z, \beta, \tau)$

$$u(\zeta, \eta, \tau) = \frac{I(z, \beta, \tau)}{A_p A_{obj} P_0} ([z - WD]^2 + z_0^2) \quad (11)$$

This substitution was made to maintain numerical stability of the system near the focal plane, where the light intensity becomes very high. The dimensionless coordinate $\eta = \beta/z_0$ appears here simply as a parameter labeling the distance of a ray from the beam center. The boundary and initial conditions for *Eqs. 9* and *10* are

$$u(z = 0, \eta, \tau) = \frac{2z_0}{\lambda} \exp\left(-2\pi \frac{z_0}{\lambda} \eta^2\right)$$

$$\hat{c}(\zeta, \eta, 0) = 1 \quad (12)$$

The equations were integrated by the implicit Euler method along 10 rays traversing the focal plane at equal distances from the beam center, out to the $1/e^2$ beam waist. The resulting radial glutamate concentration profiles were approximately Gaussian at lower powers ($\lesssim$50% conversion), but saturated centrally at higher powers ($\gtrsim$50% conversion). The corresponding spatially averaged concentrations were found to be about 5–10% higher (at lower power) or about 5% lower (at higher power) than those derived from the simplified model *Eqs. 1* and *2*. The glutamate concentration quoted in the RESULTS is the mean value over the $1/e^2$ beam radius, at $z = WD + 100$ μm, obtained from the 10 rays.

Diffusion of caged glutamate or the photoproducts during uncaging was not modeled because, at the laser powers used, radial redistribution of these compounds occurs much more slowly than their photolysis or production. The ratio of diffusion time to photolysis time is expressed as

$$\frac{\tau_D}{\tau_{ph}} \sim \frac{W(z)^2}{2D\tau_{ph}} = \frac{0.495 Q_p E_{CG}}{\pi \varepsilon_\lambda N_A D} P_0 A_p A_{obj} 10^{-E_{CG} C_0 z} \quad (13)$$

where D ($\sim 5 \times 10^{-6}$ cm^2 s^{-1}) is the diffusion coefficient of caged glutamate or photoproduct estimated from the molecular weight (Longsworth 1953). Along the beam path, the minimum ratio is attained at the cell, 100 μm below the focal plane, where τ_D/τ_{ph} is about 14 for the MNI-cage and about 34 for the NI-cage. The corresponding ratios for glutamate, obtained by multiplying by 5/7.6 (ratio of diffusion coefficients, D/D_{GLU}), are also $\gg 1$.

Extinction coefficients of pharmacological agents were determined by using a photodiode to measure the attenuation of the laser beam directed through a 10-cm cuvette containing the drugs at various concentrations. At the experimental concentrations, UV absorption was negligible for all compounds except for 10 μM NBQX (E_{NBQX} = 9,620 M^{-1} cm^{-1}) and 100 μM SYM2206 ($E_{SYM2206}$ = 5,600 M^{-1} cm^{-1}). Where appropriate, data were compensated for absorption either by boosting the laser power to a level calculated to equalize the mean concentration of released glutamate, or post hoc by applying a correction factor measured from the laser intensity dependency of the responses in the presence of the drug.

An upper bound on the time course of glutamate at the soma after flash photolysis was estimated by assuming that its removal is dominated by diffusion. Perfusion was switched off during data acquisition, to prevent bulk flow from influencing the time course of glutamate removal. If the beam released an approximately Gaussian initial distribution of glutamate with SD $\sigma = W/2 = 8.6$ μm, the concentration at the center, $C(t)$, decays as

$$C(t) \sim \frac{1}{1 + \frac{2D_{GLU} t}{\sigma^2}} C(0) \quad (14)$$

This is an upper bound because active uptake mechanisms in the slice may accelerate the removal of glutamate.

RESULTS

Caged glutamate photolysis activates NMDA receptors on mitral cells

In zero Mg^{2+} ACSF, in the presence of 1 μM TTX, 50 μM bicuculline, and 150 μM Cd^{2+}, uncaging glutamate onto the soma of a mitral cell activated a large inward current at a negative holding potential of −72.2 mV. The current was not evoked when cells were exposed to a flash in the absence of caged glutamate. The inward current began with a fast initial phase, which desensitized rapidly, followed by a much slower component that gradually decayed over many seconds (Fig. 1*A*). Addition of 10 μM NBQX to the bath eliminated the fast component (10-ms charge transfer reduced to 16 ± 7% of control, mean ± SD, $P < 0.05$, $n = 3$), indicating that it was mediated by AMPA/kainate receptors (Fig. 1, *A* and *B*). In 0 Mg^{2+}, 10 μM NBQX, the slow component evoked by uncaging glutamate (mean concentration 690 μM) was characterized by a peak amplitude of 150.7 ± 81.8 pA, a rise time of 64.2 ± 24.81 ms, a 10-s charge transfer of 1,018.5 ± 485.8 pC, and a decay at 10 s to 0.55 ± 0.17 of peak ($n = 6$).

The slow component was sensitive to antagonists of NMDA receptors. Addition of 100 μM of the competitive NMDA-receptor antagonist APV to the bath attenuated the peak of the slow component to 53 ± 7% of control ($P < 0.05$, $n = 5$), but there remained a significant inward current with peak ampli-

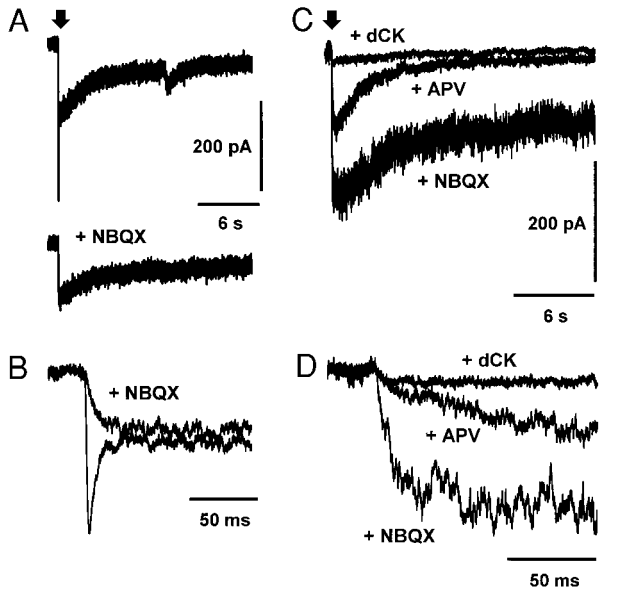

FIG. 1. NMDA receptor component of mitral cell response to flash photolysis of caged glutamate. *A*: *top trace*: fast and slow inward currents recorded in response to uncaging glutamate (MNI, 1.18 mW at cell, 680 μM) on mitral cell somatodendritic membrane, under whole cell voltage clamp in standard ACSF with 0 Mg^{2+} (−72.2 mV, $CsMeSO_3$ internal solution). Smaller spontaneous event on tail was not direct response to flash photolysis. *Bottom trace*: slow inward current remaining after application of 10 μM NBQX to block AMPA/kainate receptors. Bath contained: 1 μM TTX, 50 μM bicuculline methiodide, 150 μM Cd^{2+}. *B*: fast initial phases of responses in *A*, plotted on expanded time scale to show that application of NBQX abolished fast component. Vertical scale bar same as for *A*. *C*: superimposed traces showing photolysis responses (MNI, 1.12 mW at cell, 660 μM glutamate) recorded in presence of 10 μM NBQX, 0 Mg^{2+}, before (*bottom trace*) and after (*middle trace*) addition of 100 μM APV. Current in APV was then further attenuated by addition of 15 μM dCK (*top trace*). *D*: initial phases of the responses in A, plotted on expanded time base. Vertical scale bar same as for *C*. Arrows in *A* and *C* indicate timing of laser flash (3.5 ms).

tude 101.5 ± 26.2 pA ($n = 5$) (Fig. 1*C*). This exhibited a slower rise time of 256.6 ± 53.1 ms ($n = 7$); the addition of APV extended the rise time by 3.76 ± 1.49-fold ($P < 0.005$, $n = 5$) (Fig. 1*D*). The current in APV also decayed more rapidly, falling to 50% of its peak value in 2.01 ± 0.61 s ($n = 5$), and by 10 s it was reduced to 12 ± 7% of peak ($n = 5$). The large differences in the decay time courses are underscored by the 10-s charge transfers, which were reduced to 32 ± 18% of control by the addition of APV ($P < 0.01$, $n = 5$). The slowly decaying APV-sensitive component was also observed in physiological (1.3 mM) Mg^{2+}: addition of APV attenuated the 10-s charge transfer from 210.6 ± 114.7 to 49.8 ± 56.5 pC, and the 10-s fractional decay from 0.44 ± 0.17 to 0.13 ± 0.06 ($n = 2$).

The response in APV was strongly blocked by the addition of 15 μM dCK, a competitive antagonist of the NMDA-receptor at the glycine binding site (Fig. 1, *C* and *D*). Peak amplitude was attenuated to 22 ± 10% of control ($P < 0.01$, $n = 4$), and the 10-s charge transfer to 18 ± 9% of control ($P < 0.01$, $n = 4$). A small residual current of 19 ± 5 pA ($n = 3$) persisted in the presence of both AMPA/kainate and NMDA-receptor antagonists, which may be attributed to incomplete blockade by competitive antagonists of the response to the high glutamate concentration. The observed pharmacology suggests that the slow responses recorded in the presence of NBQX are mediated by NMDA receptors. A hallmark of NMDA receptors is their voltage-dependent blockade by extracellular Mg^{2+}. Figure 2, *A* and *B* shows the voltage dependency of the response in APV, recorded in 1.3 mM external Mg^{2+}. The current–voltage relation was nearly linear at positive holding potentials, reversed near 0 mV, and exhibited strong outward rectification at negative holding potentials, as expected from Mg^{2+} block. In APV the peak current at −72.2 mV (26.23 ± 1.74 pA; $n = 2$) was significantly reduced ($P < 0.02$) in 1.3 mM Mg^{2+} relative to 0 Mg^{2+} (94.84 ± 24.97 pA; $n = 4$).

The substantial glutamate-activated current remaining in 100 μM APV is reminiscent of the "APV-resistant" response reported from mitral cells stimulated by iontophoretic application of glutamate (Didier et al. 2001). In that study the failure of APV to block the glutamate response was interpreted as evidence for a novel NMDA receptor, one that is not antagonized by APV. However, APV may be ineffective because of competition by high concentrations of glutamate. The slowed rise and accelerated decay of the attenuated response to uncaged glutamate observed in 100 μM APV suggests a competition mechanism (Clements and Westbrook 1994). To test this pos-

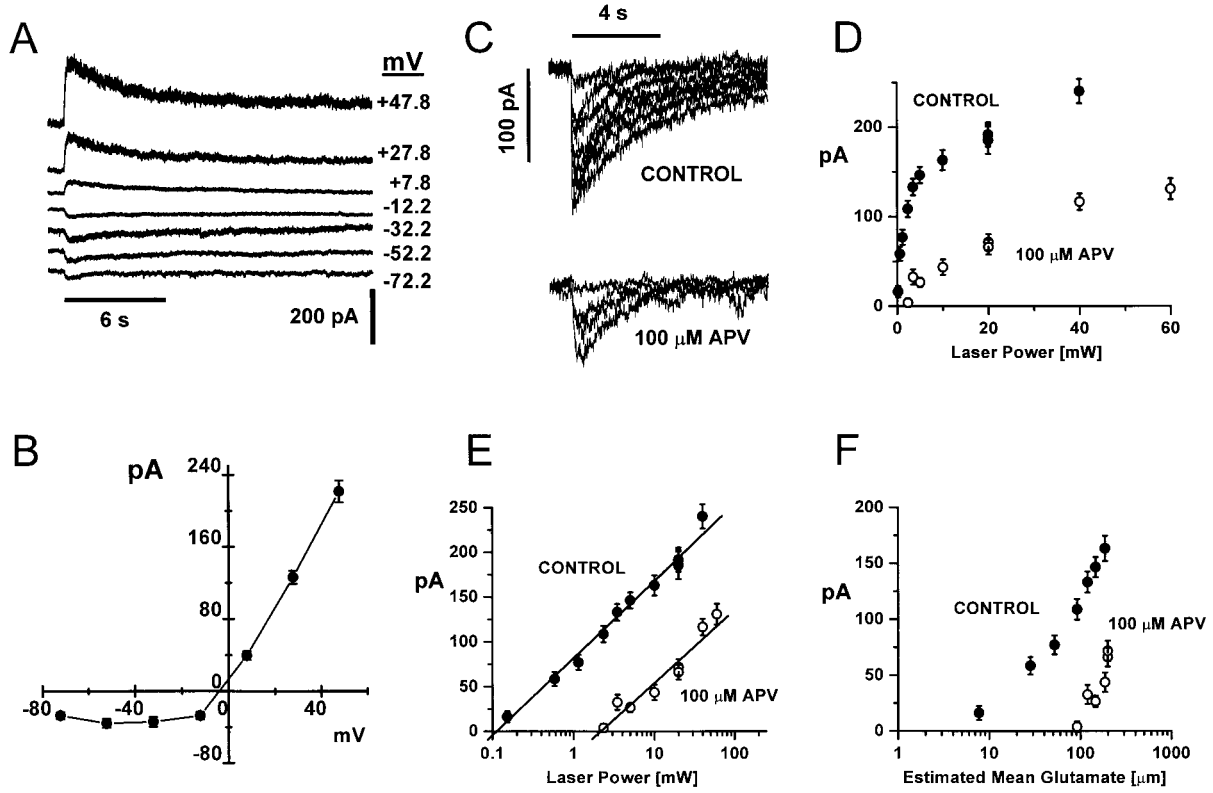

FIG. 2. Competitive inhibition of NMDA receptor current by APV. *A*: currents recorded in 1.3 mM Mg^{2+}, 100 μM APV, in response to uncaging glutamate (MNI, 7.34 mW at cell, 490 μM) at different holding potentials, which include correction for pipette liquid junction potential. Laser flash duration: 3.5 ms. *B*: current–voltage plot of peak amplitudes of responses shown in *A*, showing outward rectification. *C*: currents recorded in 0 Mg^{2+}, −72.2 mV, in response to varying concentrations of glutamate uncaged by flashes of varying intensity (MNI, 0.04–11.15 mW at cell, 7.7–200 μM), before (*top traces*) and after (*bottom traces*) addition of 100 μM APV. For clarity several *intermediate traces* were omitted from lower plot. *D*: peak amplitudes of the families of responses in *C*, plotted against laser power P_0. *E*: linear–log plots of the data in *D*. Lines were drawn by linear regression. *F*: linear–log plots of the peak amplitudes in *D*, against concentration of uncaged glutamate (average across the $1/e^2$ beam radius) calculated from photolysis model. Vertical asymptote on right, at 200 μM, is artifact of photolysis saturation (bath contained 200 μM caged glutamate) combined with continued increase of response expected from spatial summation of current from dendritic receptors. For clarity saturated points at 200 μM ($P_0 > 20$ mW) were not plotted. In all experiments, bath contained: 1 μM TTX, 50 μM bicuculline methiodide, 150 μM Cd^{2+}, 10 μM NBQX.

sibility, dose–response curves were constructed by varying the flash intensity during photolysis of a lower bath concentration (200 μM) of MNI-caged glutamate. The intensity dependency of the response, before and after addition of 100 μM APV, is shown in Fig. 2*C*, and the corresponding peak amplitudes are plotted in Fig. 2*D*. The same amplitudes are plotted against logarithmic scales of intensity (Fig. 2*E*), and spatially averaged glutamate concentration estimated from the photolysis model (Fig. 2*F*). These data clearly show that APV shifted the dose–response curves to the right, while preserving their slopes (ratio of APV/no-APV linear–log slopes, 0.94 $\pm$ 0.19, $n = 3$ cells). At lower laser powers ($\lesssim$100 μM estimated mean glutamate) the response was strongly blocked by 100 μM APV. This behavior is expected from competitive inhibition of a single high-affinity NMDA receptor; it is inconsistent with the presence of a second APV-resistant subtype of NMDA receptor on the mitral cell.

The EC_{50} values for glutamate cannot be read directly from Fig. 2, *E* and *F* because the linear–log intensity–response curves continue to rise at higher powers without clear saturation. This behavior is not surprising because the receptor dose–response curves are smeared by spatial convolution of the glutamate profile with an undetermined receptor distribution on the soma and proximal dendrites. Photolysis model calculations show that additional receptors on the dendrites will be recruited as the outer edges of the laser spot become brighter at higher power. A higher density of reciprocal synapses on the dendrites has been reported (Mori 1987), and this could correlate with a higher density of dendritic autoreceptors. Glutamate diffusion and receptor desensitization may also affect the peak amplitudes of these slow responses. However, a rough confirmation of the calculated concentrations of uncaged glutamate C_{GLU}, corresponding to about 50% inhibition by APV, can be obtained from a Cheng–Prusoff equation (Cheng and Prusoff 1973) for two identical, independent glutamate binding sites on the NMDA receptor (Benveniste and Mayer 1991; Clements and Westbrook 1991)

$$K_I = \frac{IC_{50}}{(\sqrt{2} - 1)\left(1 + \frac{C_{GLU}}{K_d}\right)} \quad (15)$$

Taking $IC_{50} = 100$ μM, and microscopic dissociation constants $K_I = 1.93$ μM for APV (Benveniste and Mayer 1991) and $K_d = 1.1$ μM for L-glutamate (Patneau and Mayer 1990), yielded $C_{GLU} \cong 140$ μM, which is consistent with the approximately 100–200 μM range estimated from photolysis modeling to bracket an approximately twofold attenuation of the response.

The AMPA/kainate component of the glutamate response

To isolate the AMPA/kainate component of the response, recordings were made with 1.3 mM Mg^{2+}, 100 μM APV, and 30 μM dCK present in the bath solution to block the slow NMDA-receptor component (Fig. 3*A*, *top trace*). Under these conditions, the current activated by uncaging glutamate onto the soma displayed a rapid onset with millisecond rise times and large amplitudes of a few hundred picoamperes (Table 1). The decay was rapid, with the amplitude falling to 50% of peak within <10 ms, and then followed a much slower time course (time constant 0.78 $\pm$ 0.13 s, monoexponential fit over 2-s interval, $n = 5$). Data were also acquired from a larger sample of cells, in the presence of APV but absence of dCK, and the fast kinetic parameters were similar except for a somewhat

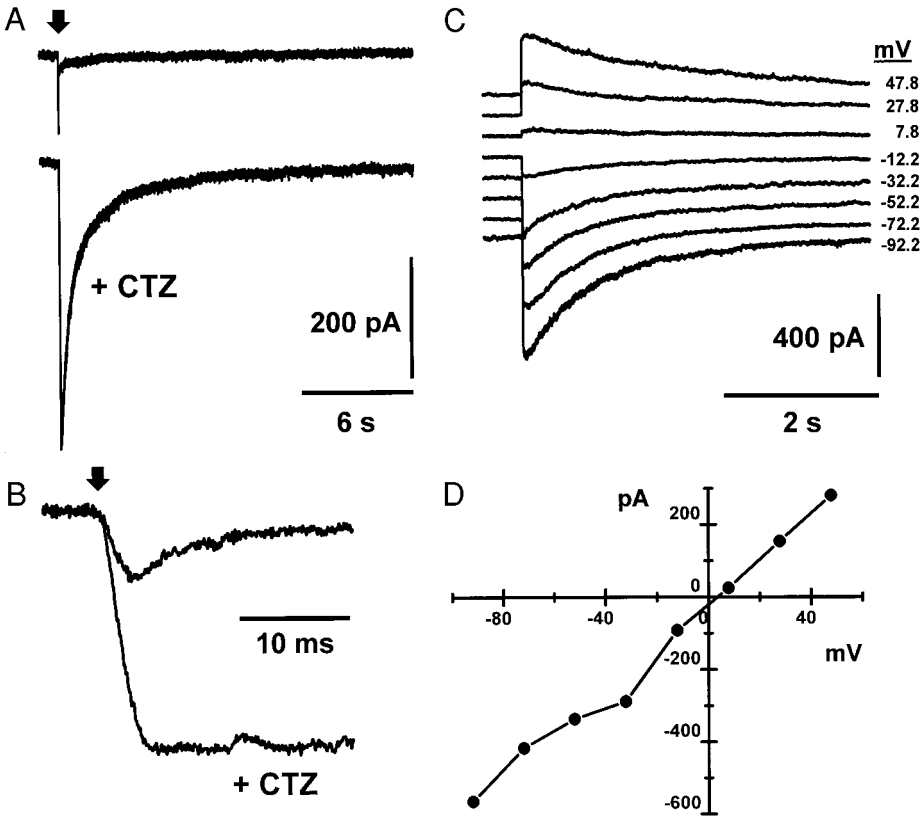

FIG. 3. Cyclothiazide potentiates AMPA/kainate component of glutamate response. *A*: inward currents recorded in response to uncaging glutamate (MNI, 1.18 mW at cell, 690 μM) before (*top trace*) and after (*bottom trace*) addition of 100 μM cyclothiazide. Bath contained: 1.3 mM Mg^{2+}, 1 μM TTX, 50 μM bicuculline methiodide, 150 μM Cd^{2+}, 100 μM APV, 30 μM dCK. *B*: initial phases of responses in *A*, plotted on expanded time base. Arrows in *A* and *B* indicate timing of laser flash. Vertical scale bar same as for *A*. *C*: cyclothiazide-potentiated current recorded at different holding potentials. *D*: current–voltage plot of peak amplitudes of responses shown in *C*.

TABLE 1. *Properties of the fast component of the glutamate response*

	With 30 μM dCK (n = 7)	Without dCK (n = 11)
	490–690 μM Glutamate	610–690 μM Glutamate
Rise time (ms)	3.41 ± 0.64	3.25 ± 0.58
50% Rise time (ms)	2.07 ± 0.47	1.84 ± 0.22
10–90% Rise time (ms)	2.37 ± 0.18	2.06 ± 0.29
10–90% Slope (pA ms^{-1})	30.09 ± 44.09	75.27 ± 44.40
Peak amplitude (pA)	145.74 ± 37.62	181.75 ± 84.82
10 ms Charge transfer (pC)	0.93 ± 0.27	1.05 ± 0.45
50% Decay time (ms)	7.53 ± 3.52	4.62 ± 1.52

Amplitudes, charge transfers, and kinetic parameters characterizing the fast transient current activated by uncaging glutamate, in the presence or absence of 5,7-dichlorokynurenate (dCK). Values are means ± SD. Corrected holding potential was −72.2 mV; bath solution contained 1.3 mM Mg^{2+} and 100 μM APV, and no cyclothiazide was added.

shorter decay time (Table 1). The NMDA-receptor current in APV rises too slowly (~260 ms) to make a significant contribution to these fast kinetic parameters. The rapid decay of the fast current is governed largely by receptor desensitization because the postflash concentration of glutamate at the soma is expected to be nearly constant within this time frame (diffusion only decreases it to 83% of initial concentration after 10 ms; cf. *Eq. 14*). Indeed, the magnitude and duration of the fast responses were strongly potentiated by the addition of 100 μM CTZ, a positive allosteric modulator of AMPA receptor desensitization (Sun et al. 2002) (Fig. 3, *A* and *B*). CTZ boosted the peak amplitude by a factor of $\beta_{CTZ} = 3.28 \pm 0.34$ ($P < 0.05$, $n = 4$), and the rise time was correspondingly lengthened by 3.07 ± 1.33-fold ($P < 0.05$, $n = 4$). The rapid decay of the response was prevented by CTZ, the 50% decay time being increased by 122 ± 67-fold (mean time 605 ± 75 ms; $P < 10^{-5}$, $n = 4$). The current–voltage relation of the response in CTZ (Fig. 3, *C* and *D*) displayed no outward rectification (Patneau et al. 1993) and reversed near 0 mV. These properties are characteristic of currents mediated by AMPA receptors.

Although potentiation by CTZ is selective for AMPA receptors (Partin et al. 1993), it is possible that the fast response also includes contributions from kainate receptors. This possibility was tested by applying the dihydrophthalazine, SYM2206, a potent ($IC_{50} = 2.8$ μM) noncompetitive allosteric inhibitor that selectively antagonizes AMPA receptors (Li et al. 1999; Pelletier et al. 1996). Inclusion of 100 μM SYM2206 in the bath attenuated the photolysis response (peak amplitude to 60 ± 14% of control; 10-ms charge transfer to 58 ± 13% of control, $P < 0.05$, $n = 8$), but a substantial fast current remained (Fig. 4, *A* and *B*). This measurement shows that a fraction, $f_{AMPA} \cong 0.4$, of the AMPA/kainate current is carried by AMPA receptors; hence the specific potentiation of the AMPA-receptor current by CTZ is $1 + (\beta_{CTZ} - 1)/f_{AMPA} \cong 1 + 2.28/0.4 \cong 6.7$. The peak amplitude in SYM2206 ranged from 25 to 210 pA (64.93 ± 49.73 pA, 200–323 μM glutamate, $n = 12$). The kinetics were not significantly altered by SYM2206: the rise time was 3.98 ± 0.97 ms (ratio 1.03 ± 0.25, $P > 0.5$), and the 50% decay time 7.57 ± 5.79 ms (ratio 1.29 ± 0.63, $P > 0.2$, $n = 8$). Because a concentration of 100 μM SYM2206 is sufficient for maximal blockade of AMPA receptors, the remaining fast current may be attributed to kainate receptor activation. This was confirmed by the addition of 10 μM NBQX, which blocked 66% of the SYM2206-resistant current

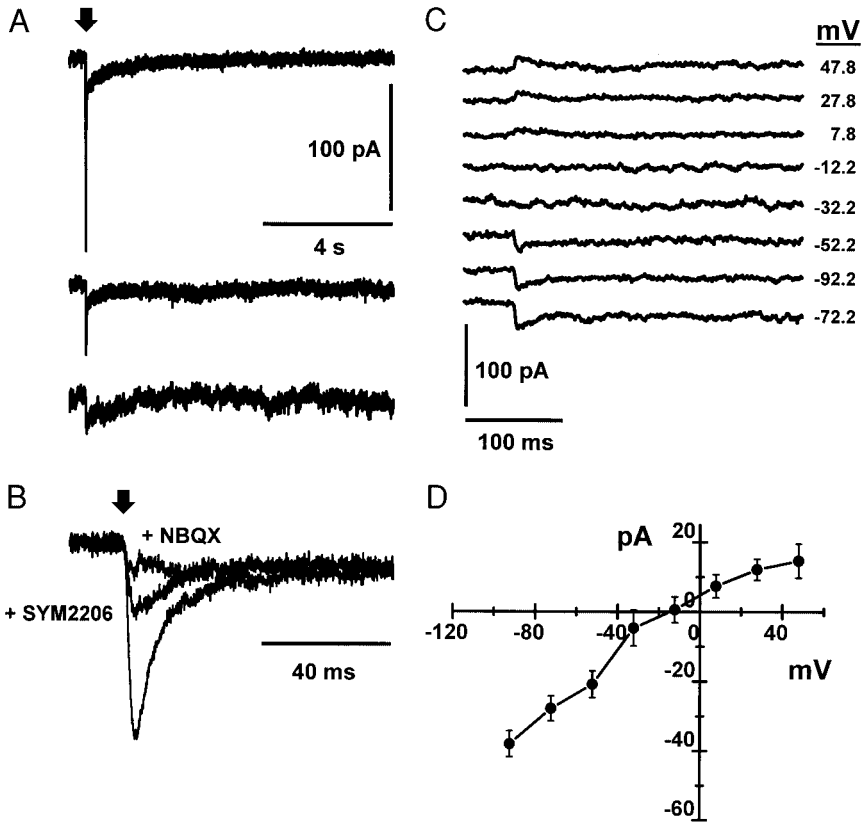

FIG. 4. Kainate receptor component of mitral cell response to flash photolysis of caged glutamate. *A*: inward currents recorded in response to uncaging glutamate (7.73 mW at cell, 490 μM) before (*top trace*) and after (*middle trace*) addition of 100 μM SYM2206. Current was further attenuated by addition of 10 μM NBQX (*top trace*). Bath contained: 1.3 mM Mg^{2+}, 1 μM TTX, 50 μM bicuculline methiodide, 150 μM Cd^{2+}, 100 μM APV, 30 μM dCK. *B*: initial phases of responses in *A*, plotted on expanded time base. Arrows in *A* and *B* indicate timing of laser flash. Vertical scale bar same as for *A*. *C*: kainate receptor component of photolysis response recorded at different holding potentials. *D*: current–voltage plot of peak currents of responses shown in *C*.

(peak amplitude reduced to 34 ± 9% of control, $n = 3$) (Fig. 4, *A* and *B*). The current–voltage relation of the SYM2206-resistant current was approximately linear and reversed near the origin (Fig. 4, *C* and *D*).

DISCUSSION

In this study flash photolysis was used to probe the glutamate sensitivity of the mitral cell soma and proximal dendrites. Photorelease of several hundred micromolar glutamate activated a large excitatory conductance. Selective pharmacological blockade demonstrated that this conductance included major contributions from AMPA, kainate, and NMDA classes of ionotropic glutamate receptors.

Initial evidence for the expression of ionotropic glutamate receptors on the somatodendritic membrane of mitral cells came from immunocytochemical studies. Mitral somata and secondary dendrites in the external plexiform layer were strongly labeled by antibodies to AMPA receptor subunits GluR1 and GluR2/3, kainate receptor subunits GluR5/6/7 (Hamilton and Coppola 2003; Montague and Greer 1999), and NMDA receptor subunit NR1 (Giustetto et al. 1997; Watanabe et al. 1993). The results presented here confirm the functional expression of these classes of ionotropic glutamate receptors on the mitral cell. However, a high-resolution immunogold study found NR1 and GluR2/3 subunit labeling only on the granule cell side of dendrodendritic synapses (Sassoe-Pognetto and Ottersen 2000), and it was suggested that glutamate autoreceptors on the mitral cell escaped detection because they occur at low density. The somatodendritic AMPA receptor conductance activated by uncaging approximately 500–700 μM glutamate is about 2.9 nS (at −72.2 mV, average AMPA receptor current in CTZ is about $0.4 \times 3.3 \times 160$ pA = 210 pA). Assuming a single-channel conductance of about 8 pS (Ascher and Nowak 1988), an open probability of about 0.50 (Diamond and Jahr 1997), and a somatic diameter of about 25 μm, the average AMPA receptor density is about 0.4 μm^{-2}, which is indeed low compared with, for instance, cultured hippocampal neurons with extrasynaptic density of about 3 μm^{-2} (Cottrell et al. 2000). However, the local density may be higher if AMPA receptors are concentrated at dendrodendritic synapses.

The lack of asymmetric synapses directed onto the mitral soma and dendrites in the external plexiform layer suggested that glutamate receptors there may function as autoreceptors, detecting glutamate released from the mitral cell during dendrodendritic transmission. Self-excitation of mitral cells was originally observed in vivo in the turtle olfactory bulb, where blockade of $GABA_A$ receptors unmasked a strong depolarizing afterpotential after spike discharge (Nicoll and Jahr 1982). This potential was blocked by Cd^{2+} and a glutamate receptor antagonist, suggesting that it represented the response of the mitral cell to release of its own transmitter. More recently, spike-induced autoexcitation was reported in slices of rat olfactory bulb in low extracellular Mg^{2+} (Aroniadou-Anderjaska et al. 1999; Friedman and Strowbridge 2000). These slow depolarizing responses were abolished by APV, indicating mediation by NMDA receptors, but were unaffected by NBQX. However, an NBQX-sensitive response to AMPA stimulation of the secondary dendrites indicated the presence of functional AMPA/kainate receptors (Friedman and Strowbridge 2000). Another study implicated both NMDA and AMPA/kainate receptors in autoexcitation (Salin et al. 2001). Slow autoexcitatory responses were resolved into APV- and NBQX-sensitive components. The decay time of the NBQX-sensitive component was relatively long (~60 ms) for AMPA receptors, which usually desensitize within <15 ms (Colquhoun et al. 1992; Hausser and Roth 1997), and it was suggested that the slow decay may be attributed to kainate receptors. In this study the finding of a substantial NBQX-blockable photolysis response that was insensitive to the AMPA receptor-specific antagonist SYM2206 provides further evidence for functional expression of kainate receptors on mitral cells. The fast currents seen here did not include a slow 60-ms decay. However, a much longer tail current (0.79 s) persisted in NBQX and NMDA-receptor antagonists, which may represent competitive activation of NMDA receptors by high concentrations of uncaged glutamate.

The photolysis method is ideally suited to the measurement of the fast AMPA/kainate current, which is not easily resolved in recordings of voltage pulse- or action potential-evoked autoexcitation, as a consequence of temporal overlap with imperfectly cancelled whole cell capacitance transients, or unclamped regenerative Na^+ and Ca^{2+} currents (Salin et al. 2001). Its rapid kinetics, voltage dependency, susceptibility to NBQX, modulation by CTZ, and antagonism by SYM2206 are consistent with properties of AMPA/kainate responses characterized in many other cell types (Ozawa et al. 1998). The rise time of the fast component matched the 3.5-ms shutter open time, which sets the duration of photolysis. The approximately threefold extension of the rise time in CTZ might be attributable to postphotolysis recruitment of additional AMPA receptors by radial diffusion of glutamate. Diffusion would normally be too slow to recruit rapidly desensitizing receptors, but it can do so when desensitization is blocked.

What is the role of the fast AMPA/kainate current? It is unlikely to exert much influence on membrane potential when activated by glutamate released by an action potential. At physiological temperatures, fast transmitter release in the mammalian CNS commences just 150 μs after action potential onset, so glutamate release would overlap the spike waveform (Sabatini and Regehr 1996). In this time frame, an AMPA/kainate self-excitation current of a few hundred picoamperes should be overwhelmed by large regenerative spike currents in the nanoampere range. Indeed, control experiments found no effect of 10 μM NBQX on the spike waveform in mitral cells (data not shown). However, the fast autoexcitatory current might act to boost the resting excitability of mitral cells by operating a positive feedback loop, one that is active in the subthreshold state attributed to spontaneous vesicle fusion at the mitral somatodendritic membrane. Spontaneously released packets of glutamate could generate AMPA/kainate autoreceptor excitatory postsynaptic potentials (EPSPs), which locally unblock NMDA autoreceptors, allowing them to respond more slowly to lower concentrations of glutamate as it dissipates by diffusion. Such tonic excitation may serve to oppose or cancel tonic inhibition arising from spontaneously released GABA from granule cell spines.

Previously, the glutamate sensitivity of the mitral soma and secondary dendrites was probed directly by iontophoretic application of glutamate (Didier et al. 2001). In the presence of NBQX, iontophoresis activated a large depolarizing current

insensitive to APV. This contrasted with the nearly complete blockade by APV of autoexcitatory currents evoked by direct depolarization of mitral cells. To explain these results, the authors proposed an unconventional model of mitral cell excitation involving two spatially segregated subtypes of NMDA receptors: APV-resistant receptors on the mitral cell membrane and APV-sensitive receptors restricted to glutamate-releasing granule cell spines that make reciprocal synaptic contacts with mitral cells. During self-excitation, the two receptors would work in series: glutamate released from a mitral cell would activate APV-sensitive receptors on the spines, which would in turn release glutamate to activate APV-resistant receptors on the mitral cell. The APV-sensitive receptors were confined to the synaptic cleft (to explain their activation by synaptic transmission, but not iontophoresis), whereas the APV-resistant receptors were also located extrasynaptically (and hence accessible to iontophoresis). The model was supported by immunogold labeling of spines by antibodies to glutamate-glutaraldehyde conjugates in fixed tissue, and observation of mitral cell EPSCs sensitive to ionotropic glutamate receptor blockers during iontophoretic stimulation of the granule cell layer.

The use of caged glutamate provides a rigorous test of this model. Photolytically liberated glutamate bypasses diffusional barriers presented by the geometry of the synaptic cleft and perisynaptic transporters (Corrie et al. 1993), permitting direct activation of both APV-sensitive and putative APV-resistant receptors. The dose–response relation obtained with varying levels of photolysis shows that the glutamate sensitivity of mitral cells in NBQX, and its antagonism by APV, can be explained by competitive inhibition of high-affinity NMDA receptors. The APV-resistant NMDA receptor appears to be an artifact of competition by high glutamate concentrations. Accordings to Ficks law (Carslaw and Jaeger 1959; Dionne 1976), an iontophoretic current I of duration t applies a glutamate concentration of

$$C_{\mathrm{GLU}}(r, t) = \frac{nI}{4\pi zFD_{\mathrm{GLU}}r}\,\mathrm{erfc}\left(\frac{r}{2\sqrt{D_{\mathrm{GLU}}t}}\right) \qquad (16)$$

to the membrane at a distance r from the pipette tip. Typical experimental parameters were as follows: $r \cong 25\ \mu$m, $t = 0.5$ s, $I \cong -300$ nA (Didier et al. 2001); $F = 96{,}485$ cmol^{-1}; the transport number is assumed to be $n \cong 0.5$ for a pure solution of Na-glutamate, with $z = -1$ the ionic valence of 96.8% of the glutamate titrated to pH 8.2; these numbers give: $C_{\mathrm{GLU}} \cong 2.4$ mM. At this concentration, the two-site model of the NMDA receptor predicts 87–95% maximal activation in 300–100 μM APV. This could explain much of the insensitivity of the iontophoretic responses to APV.

The dendrodendritic excitation model also requires that the APV-sensitive component of the mitral cell response to uncaged glutamate be mediated by glutamate-induced glutamate release from granule cell spines. Transmitter release is a highly cooperative function of depolarization-induced calcium influx (Augustine and Charlton 1986), but no sign of positive cooperativity is evident in the control intensity–response (Fig. 2*E*) or glutamate–response curves (Fig. 2*F*). Log–log plots of the glutamate–response curves near threshold, where they are fully blocked by APV, yielded slopes of 0.60 ± 0.04 ($n = 3$).

The findings of this study argue against the punctate dendrodendritic excitation model, and imply that self-excitation of the mitral cell somatodendritic membrane depends exclusively on autoreceptor activation. Because of their rapid desensitization and low affinity, the AMPA/kainate autoreceptors would need to be localized close to release sites to be functional (i.e., within or near the cleft of the dendrodendritic inhibitory synapses). On the other hand, a fraction of the slow, high-affinity NMDA autoreceptors may be deployed extrasynaptically, where they may detect glutamate spillover under conditions of enhanced transmitter release (Isaacson 1999), such as during concerted high-frequency firing of locally excited populations of mitral and granule cells. Under such conditions, sufficient glutamate may be released to saturate uptake mechanisms and activate NMDA autoreceptors in coincidence with relief of Mg^{2+} blockade by somatic and backpropagating dendritic action potentials (Lowe 2002; Margrie et al. 2001; Xiong and Chen 2002). Repetitive activity seems to be able to release enough glutamate at mitral cell axon collaterals to activate extrasynaptic NMDA receptors on granule cells (Isaacson and Murphy 2001). Spatial clustering of reciprocal synapses along the secondary dendrites (Lowe 2002) may enhance self-excitation by creating local spillover domains of elevated extrasynaptic glutamate.

In the olfactory bulb, lateral inhibitory circuits constructed from bidirectional excitatory–inhibitory synapses offer the advantages of a compact, economical architecture. A lateral inhibitory network built from conventional one-way synapses would require twice as many interneurons to achieve the same functionality. However, the use of bidirectional synapses entails the additional complexity of negative feedback inhibition. Such negative feedback is usually considered an important pathway for the temporal patterning of mitral cell discharge during olfactory information processing. However, it also limits the frequency and duration of firing patterns available to mitral cells. Positive feedback loops implemented by autoreceptors may have evolved to balance and regulate this negative feedback, and expand the dynamic range of signaling available to the dendrodendritic network.

The author gratefully acknowledges helpful comments and advice on the manuscript from A. Gelperin, B. M. Salzberg, and D. J. Perkel. Unpublished data on molar extinction coefficients of nitrosoindole photoproducts were generously provided by J. E. T. Corrie. Invaluable technical assistance in the laboratory was provided by A. Ladavac.

DISCLOSURES

This work was supported by National Institute on Deafness and Other Communication Disorders Grant RO1 DC-04208-02.

REFERENCES

Aroniadou-Anderjaska V, Ennis M, and Shipley MT. Dendrodendritic recurrent excitation in mitral cells of the rat olfactory bulb. *J Neurophysiol* 82: 489–494, 1999.

Ascher P and Nowak L. Quisqualate- and kainate-activated channels in mouse central neurones in culture. *J Physiol* 399: 227–245, 1988.

Augustine GJ and Charlton MP. Calcium dependence of presynaptic calcium current and post-synaptic response at the squid giant synapse. *J Physiol* 381: 619–640, 1986.

Barry PH. JPCalc, a software package for calculating liquid junction potential corrections in patch-clamp, intracellular, epithelial and bilayer measurements and for correcting junction potential measurements. *J Neurosci Methods* 51: 107–116, 1994.

Benveniste M and Mayer ML. Kinetic analysis of antagonist action at *N*-methyl-D-aspartic acid receptors. Two binding sites each for glutamate and glycine. *Biophys J* 59: 560–573, 1991.

Berkowicz DA, Trombley PQ, and Shepherd GM. Evidence for glutamate as the olfactory receptor cell neurotransmitter. *J Neurophysiol* 71: 2557–2561, 1994.

Canepari M, Nelson L, Papageorgiou G, Corrie JE, and Ogden D. Photochemical and pharmacological evaluation of 7-nitroindolinyl- and 4-methoxy-7-nitroindolinyl-amino acids as novel, fast caged neurotransmitters. *J Neurosci Methods* 112: 29–42, 2001.

Carslaw HS and Jaeger JC *Conduction of Heat in Solids* (2nd ed). Oxford University Press, 1959.

Cheng Y and Prusoff WH. Relationship between the inhibition constant (K_i) and the concentration of inhibitor which causes 50 per cent inhibition (I_{50}) of an enzymatic reaction. *Biochem Pharmacol* 22: 3099–3108, 1973.

Clements JD and Westbrook GL. Activation kinetics reveal the number of glutamate and glycine binding sites on the *N*-methyl-D-aspartate receptor. *Neuron* 7: 605–613, 1991.

Clements JD and Westbrook GL. Kinetics of AP5 dissociation from NMDA receptors: evidence for two identical cooperative binding sites. *J Neurophysiol* 71: 2566–2569, 1994.

Colquhoun D, Jonas P, and Sakmann B. Action of brief pulses of glutamate on AMPA/kainate receptors in patches from different neurones of rat hippocampal slices. *J Physiol* 458: 261–287, 1992.

Corrie JET, DeSantis A, Katayama Y, Khodakhah K, Messenger JB, Ogden DC, and Trentham DR. Postsynaptic activation at the squid giant synapse by photolytic release of L-glutamate from a "caged" L-glutamate. *J Physiol* 465: 1–8, 1993.

Cottrell JR, Dube GR, Egles C, and Liu G. Distribution, density, and clustering of functional glutamate receptors before and after synaptogenesis in hippocampal neurons. *J Neurophysiol* 84: 1573–1587, 2000.

Diamond JS and Jahr CE. Transporters buffer synaptically released glutamate on a submillisecond time scale. *J Neurosci* 17: 4672–4687, 1997.

Didier A, Carleton A, Bjaalie JG, Vincent JD, Ottersen OP, Storm-Mathisen J, and Lledo PM. A dendrodendritic reciprocal synapse provides a recurrent excitatory connection in the olfactory bulb. *Proc Natl Acad Sci USA* 98: 6441–6446, 2001.

Dionne VE. Characterization of drug iontophoresis with a fast microassay technique. *Biophys J* 16: 705–717, 1976.

Ennis M, Zimmer LA, and Shipley MT. Olfactory nerve stimulation activates rat mitral cells via NMDA and non-NMDA receptors in vitro. *Neuroreport* 7: 989–992, 1996.

Friedman D and Strowbridge BW. Functional role of NMDA autoreceptors in olfactory mitral cells. *J Neurophysiol* 84: 39–50, 2000.

Getchell TV and Shepherd GM. Short-axon cells in the olfactory bulb: dendrodendritic synaptic interactions. *J Physiol* 251: 523–548, 1975.

Giustetto M, Bovolin P, Fasolo A, Bonino M, Cantino D, and Sassoe-Pognetto M. Glutamate receptors in the olfactory bulb synaptic circuitry: heterogeneity and synaptic localization of *N*-methyl-D-aspartate receptor subunit 1 and AMPA receptor subunit 1. *Neuroscience* 76: 787–798, 1997.

Hamilton KA and Coppola DM. Distribution of GluR1 is altered in the olfactory bulb following neonatal naris occlusion. *J Neurobiol* 54: 326–336, 2003.

Hausser M and Roth A. Dendritic and somatic glutamate receptor channels in rat cerebellar Purkinje cells. *J Physiol* 501: 77–95, 1997.

Isaacson JS. Glutamate spillover mediates excitatory transmission in the rat olfactory bulb. *Neuron* 23: 377–384, 1999.

Isaacson JS and Murphy GJ. Glutamate-mediated extrasynaptic inhibition: direct coupling of NMDA receptors to Ca^{2+}-activated K^+ channels. *Neuron* 31: 1027–1034, 2001.

Isaacson JS and Strowbridge BW. Olfactory reciprocal synapses: dendritic signaling in the CNS. *Neuron* 20: 749–761, 1998.

Jahr CE and Nicoll RA. Dendrodendritic inhibition: demonstration with intracellular recording. *Science* 207: 1473–1475, 1980.

Li P, Wilding TJ, Kim SJ, Calejesan AA, Huettner JE, and Zhuo M. Kainate-receptor-mediated sensory synaptic transmission in mammalian spinal cord. *Nature* 397: 161–164, 1999.

Longsworth LG. Diffusion measurements, at 25°, of aqueous solutions of amino acids, peptides and sugars. *J Am Chem Soc* 75: 5705–5709, 1953.

Lowe G. Inhibition of backpropagating action potentials in mitral cell secondary dendrites. *J Neurophysiol* 88: 64–85, 2002.

Margrie TW, Sakmann B, and Urban NN. Action potential propagation in mitral cell lateral dendrites is decremental and controls recurrent and lateral inhibition in the mammalian olfactory bulb. *Proc Natl Acad Sci USA* 98: 319–324, 2001.

Montague AA and Greer CA. Differential distribution of ionotropic glutamate receptor subunits in the rat olfactory bulb. *J Comp Neurol* 405: 233–246, 1999.

Mori K. Membrane and synaptic properties of identified neurons in the olfactory bulb. *Prog Neurobiol* 29: 275–320, 1987.

Morrison J, Wan P, Corrie JET, and Papageorgiou G. Mechanisms of photorelease of carboxylic acids from 1-acyl-7-nitroindolines in solutions of varying water content. *Photochem Photobiol Sci* 1: 960–969, 2002.

Ng B and Barry PH. The measurement of ionic conductivities and mobilities of certain less common organic ions needed for junction potential corrections in electrophysiology. *J Neurosci Methods* 56: 37–41, 1995.

Nicoll RA and Jahr CE. Self-excitation of olfactory bulb neurones. *Nature* 296: 441–444, 1982.

Ozawa S, Kamiya H, and Tsuzuki K. Glutamate receptors in the mammalian central nervous system. *Prog Neurobiol* 54: 581–618, 1998.

Papageorgiou G and Corrie JET. Effects of aromatic substituents on the photocleavage of 1-acyl-7-nitroindolines. *Tetrahedron* 56: 8197–8205, 2000.

Papageorgiou G, Ogden D, Barth A, and Corrie JET. Photorelease of carboxylic acids from 1-acyl-7-nitroindolines in aqueous solution: rapid and efficient photorelease of L-glutamate. *J Am Chem Soc* 121: 6503–6504, 1999.

Partin KM, Patneau DK, Winters CA, Mayer ML, and Buonanno A. Selective modulation of desensitization at AMPA versus kainate receptors by cyclothiazide and concanavalin A. *Neuron* 11: 1069–1082, 1993.

Patneau DK and Mayer ML. Structure-activity relationships for amino acid transmitter candidates acting at *N*-methyl-D-aspartate and quisqualate receptors. *J Neurosci* 10: 2385–2399, 1990.

Patneau DK, Vyklicky L Jr, and Mayer ML. Hippocampal neurons exhibit cyclothiazide-sensitive rapidly desensitizing responses to kainate. *J Neurosci* 13: 3496–3509, 1993.

Pelletier JC, Hesson DP, Jones KA, and Costa AM. Substituted 1,2-dihydrophthalazines: potent, selective, and noncompetitive inhibitors of the AMPA receptor. *J Med Chem* 39: 343–346, 1996.

Price JL and Powell TP. The mitral and short axon cells of the olfactory bulb. *J Cell Sci* 7: 631–651, 1970a.

Price JL and Powell TP. The synaptology of the granule cells of the olfactory bulb. *J Cell Sci* 7: 125–155, 1970b.

Rall W, Shepherd GM, Reese TS, and Brightman MW. Dendrodendritic synaptic pathway for inhibition in the olfactory bulb. *Exp Neurol* 14: 44–56, 1966.

Sabatini BL and Regehr WG. Timing of neurotransmission at fast synapses in the mammalian brain. *Nature* 384: 170–172, 1996.

Saleh BEA and Teich MC *Fundamentals of Photonics.* New York: Wiley, 1991.

Salin PA, Lledo PM, Vincent JD, and Charpak S. Dendritic glutamate autoreceptors modulate signal processing in rat mitral cells. *J Neurophysiol* 85: 1275–1282, 2001.

Sassoe-Pognetto M, Cantino D, Panzanelli P, Verdun DC, Giustetto M, Margolis FL, De Biasi S, and Fasolo A. Presynaptic co-localization of carnosine and glutamate in olfactory neurones. *Neuroreport* 5: 7–10, 1993.

Sassoe-Pognetto M and Ottersen OP. Organization of ionotropic glutamate receptors at dendrodendritic synapses in the rat olfactory bulb. *J Neurosci* 20: 2192–2201, 2000.

Schoppa NE and Westbrook GL. AMPA autoreceptors drive correlated spiking in olfactory bulb glomeruli. *Nat Neurosci* 5: 1194–1202, 2002.

Sun Y, Olson R, Horning M, Armstrong N, Mayer M, and Gouaux E. Mechanism of glutamate receptor desensitization. *Nature* 417: 245–253, 2002.

van den Pol AN. Presynaptic metabotropic glutamate receptors in adult and developing neurons: autoexcitation in the olfactory bulb. *J Comp Neurol* 359: 253–271, 1995.

Watanabe M, Inoue Y, Sakimura K, and Mishina M. Distinct distributions of five *N*-methyl-D-aspartate receptor channel subunit mRNAs in the forebrain. *J Comp Neurol* 338: 377–390, 1993.

Xiong W and Chen WR. Dynamic gating of spike propagation in the mitral cell lateral dendrites. *Neuron* 34: 115–126, 2002.